Enhanced pore space analysis by use of µ-CT, MIP, NMR, and SIP

Zeyu Zhang [1] [2], Sabine Kruschwitz [2] [3], Andreas Weller [4], Matthias Halisch [5], Carsten Prinz[2]

[1] Southwest Petroleum University, School of Geoscience and Technology, Chengdu, China
[2] Federal Institute for Material Research and Testing (BAM), D-12205 Berlin, Germany
[3] Berlin University of Technology, Institute of Civil Engineering, 13355 Berlin, Germany
[4] Clausthal University of Technology, Institute of Geophysics, D-38678 Clausthal-Zellerfeld, Germany
[5] Leibniz Institute for Applied Geophysics (LIAG), D-30655 Hannover, Germany

This paper was prepared for presentation at the International Symposium of the Society of Core Analysts held in Vienna, Austria, 27 August – 1 September 2017

ABSTRACT

We investigate the pore space of rock samples with respect to different petrophysical parameters using various methods, which provide data upon pore size distributions, including micro computed tomography (µ-CT), mercury intrusion porosimetry (MIP), nuclear magnetic resonance (NMR), and spectral induced polarization (SIP). The resulting cumulative distributions of pore volume as a function of pore size are compared. Considering that the methods differ with regard to their limits of resolution, a multiple length scale characterization of the pore space geometry is proposed, that is based on a combination of the results from all of these methods. The findings of this approach are compared and discussed by using Bentheimer sandstone. Additionally, we compare the potential of SIP to provide a pore size distribution with other commonly used methods (MIP, NMR). The limits of resolution of SIP depend on the usable frequency range (between 0.002 and 100 Hz). The methods with similar resolution show a similar behavior of the cumulative pore volume distribution in the overlapping pore size range. The methods µ-CT and NMR provide the pore body size while MIP and SIP characterize the pore throat size. Using this difference, the average pore body to throat ratio is determined to be about three for the Bentheimer sandstone.

Our study shows that a good agreement between the pore radii distributions can only be achieved if the curves are adjusted considering the resolution and pore volume in the relevant range of pore radii. The MIP curve with the widest range in resolution should be used as reference

INTRODUCTION

The transport and storage properties of reservoir rocks are determined by the size and arrangement of the pores. Different methods have been developed to determine the pore size distribution of rocks. These methods are based on different physical principles. Therefore, it can be expected that the methods recognize different geometries and sizes. The pore size ranges in which the methods are most sensitive are necessarily different [1].The authors of the report [2] state that no experimental method provides the absolute value of parameters such as porosity, pore size, surface area, and surface roughness. The selection of a method of characterization has to consider the type of material and the parameter of interest. A variety of studies has been performed to compare the different experiments with different aims, for example comparing capillary pressure method and NMR [3]. This study presents an approach to describe and quantify the pore space geometry of Bentheimer sandstone using methods with different resolution. One sample is investigated by µ-CT, MIP, NMR, and SIP. The resulting pore size distributions are compared.

METHODOLOGY

The experimental methods include mercury intrusion porosimetry (MIP) [4], nuclear magnetic resonance (NMR) [5], micro computed tomography (µ-CT) [6], and spectral induced polarization (SIP) [7].

µ-CT can only resolve the part of the pore space with pore sizes larger than the resolution of the µ-CT image. Considering a voxel size of 1.75 µm of the µ-CT image and a minimum extension of pores of two voxels in one direction that can be separated by the algorithm, a minimum pore size of 3.5 µm (or minimum pore radius 1.75 µm) has to be regarded as effective resolution limit of µ-CT. Therefore, the pore volume determined by µ-CT ignores the pore space with radii smaller than 1.75 µm. For this study, a GE nanotom X-ray µ-CT has been used. For pore network separation, a combination of manual thresholding and watershed algorithms is applied to achieve the qualitatively best separated pore space. Additionally, separation results have been cross checked with SEM data. More details on this digital image analysis workflow can be found in [8].

From MIP method, the entry sizes of pores and cavities can be determined according to the Washburn-equation [9]:

$$r = -\frac{2 \cdot \gamma \cdot \cos\theta}{p}, \quad (1)$$

with r being the pore throat radius, γ = 0.48 N/m the surface tension of mercury, θ = 140° the contact angle, and p the pressure. The MIP experiments have been conducted with the PASCAL 140/440 instruments from Thermo Fisher [10], which covered a pressure range between 0.015 and 400 MPa corresponding to a pore radius range from 1.8 nm to 55 µm. The resulting pore volume is regarded to be the total pore volume that is used to calculate the porosity of the sample.

From NMR, considering the capillary tube model with straight cylindrical pores of uniform radius *r*, we get the following relationship [3]:

$$r = 2\rho T_2 , \quad (2)$$

with ρ being the surface relaxivity, and T_2 the transverse relaxation time. The signal amplitude at a given relaxation time corresponds to the pore volume related to the pore radius determined by equation 2. The NMR experiments have been performed with a Magritek Rock Core Analyzer equipment operating at a Larmor frequency of 2 MHz at room temperature (~ 20°C) and ambient pressure. After drying at 35°C for more than 48 hours in vacuum, the sample is fully saturated with low conductivity brine. NMR measurements can be calibrated to get the porosity of the sample. The early time relaxation signal corresponds to the total water content. The range of pore radii depends on the value of surface relaxivity.

Another approach to derive a pore size distribution is based on the SIP method. Debye decomposition [11] is used to determine the electrical relaxation time distribution as well as the total chargeability from complex conductivity spectra. To transform the relaxation time distribution into a pore size distribution, we use the approach proposed by [12] and applied by [13] for the Stern layer polarization model:

$$r = \sqrt{2\tau D_{(+)}} , \quad (3)$$

with $D_{(+)}$ being the diffusion coefficient of the counter-ions in the Stern layer and τ being the relaxation time. Originally, this equation describes the relation between the radius of spherical particles in an electrolyte solution and the resulting relaxation time. Though it remains discussible whether the radius of spherical grains can be simply replaced by the pore radius [14], we generally follow this approach. Additionally, we assume a constant diffusion coefficient $D_{(+)} = 3.8\times10^{-12}$ m²/s as proposed by [15]. With the pore radius *r* calculated from relaxation time τ, we compile a curve showing the cumulative volume fraction as a function of pore radius. The signal amplitude at a given relaxation time corresponds to the pore volume related to the pore radius determined by equation 3.

SIP spectra were recorded using a four-electrode sample holder as described by [16]. The complex conductivity spectra were acquired with the impedance spectrometer ZEL-SIP04 [17] in the frequency range between 0.002 and 100 Hz under ambient conditions at a constant temperature of about 20 °C. The sample was fully saturated with a sodium-chloride solution with a conductivity of 100 mS/m. At least two measurements were performed for the sample to verify the repeatability. The SIP method resolves only a range of pore radii that depends on the diffusion coefficient. Using $D_{(+)} = 3.8\times10^{-12}$ m²/s in equation 3, we get a range of pore radii between 0.1 and 25 µm.

SAMPLE MATERIAL

This study investigated a Bentheimer sandstone sample BH5-2. Being exposed in outcrops just east of the Dutch-German border in the vicinity of Bad Bentheim, the shallow-marine Bentheimer Sandstone was deposited during the Early Cretaceous and forms an important reservoir rock for petroleum [18]. The sample investigated in our study is characterized by a porosity of 23 %, a permeability of 425 mD and a specific internal surface of 0.3 m²/g. Figure 1 showcases an SEM (A) image, as well as a 2D CT slice of the material (B) and a 3D view upon the pore system (C).

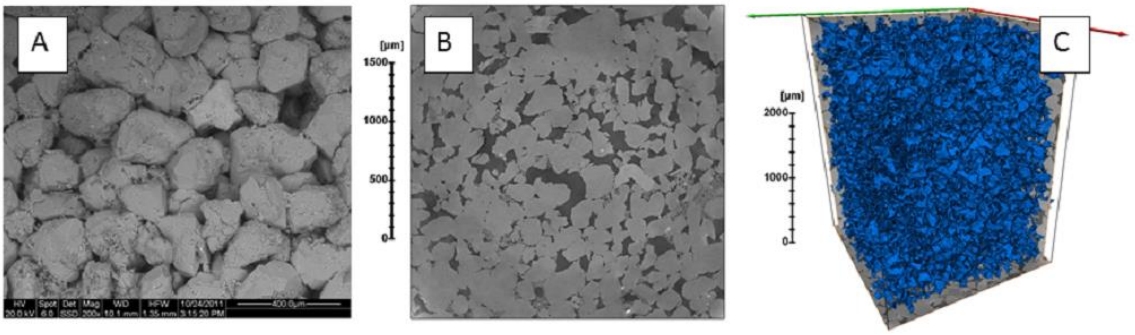

Figure 1: SEM (A) and 2D (B) and 3D (C) CT views upon the minerals and pore structure of the investigated sample of Bentheimer sandstone.

RESULTS AND DISCUSSION

The pore radius distribution is described by the relationship between the parameter V_c and the pore radius r, which is presented in a double logarithmic plot showing the relation log (V_c) versus log(r) following the procedure described in [19]. V_c represents the cumulative volume fraction of pores with radii less than r, which is expressed by

$$V_c = \frac{V(<r)}{V}, \qquad (4)$$

with V being the total pore volume, and $V(<r)$ the cumulative volume of pores with radii less than r.

The MIP curve gets a fixed position in the plot shown in Figure 2. It covers the widest range of pore radii and the full range of V_c. All other curves have to be adjusted considering the limits of the range of pore radii. The µ-CT curve uses the absolute pore radii determined by the image processing algorithm. The maximum of the µ-CT curve corresponds to $V_c = 1$ because no larger pore size has been detected by other methods. The fractional porosity of the sample as determined by MIP reaches 0.238. The porosity determined by µ-CT reaches only 0.184 (Table 1). This value corresponds to a fraction of 0.773 of the porosity determined by MIP. Therefore, the minimum of the µ-CT curve at the pore radius of 1.75 µm has been adjusted at $V_c = 1 - 0.773 = 0.227$. We observe a strong shift of the µ-CT curve to larger pore radii in comparison with MIP. This shift can be explained by the different pore geometries sensed by the two methods. MIP records the pore throat radius

that is the entry radius to fill the pores with mercury. Although MIP might not represent the true distribution of pore throats due to the restricted accessibility to the pores, the dominant pore radius of Bentheimer sandstone is relatively large so that this problem is of minor importance for this sample. The µ-CT method provides the average pore radius calculated from the equivalent pore diameter which is larger than the pore throat radius and corresponds to the average pore body radius. Considering the median pore radius at V_c = 0.5 for the two methods, we get a ratio of about three between the pore body and pore throat radius of the investigated Bentheimer sandstone sample.

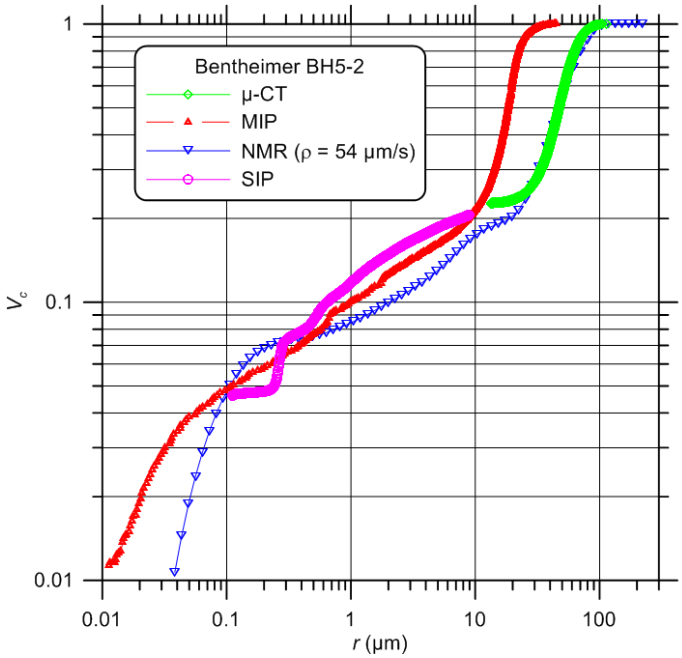

Figure 2: The comparison of V_c-r curves determined from µ-CT, MIP, NMR and SIP for sample BH5-2.

The NMR method is sensitive to the pore body radius, too. Therefore, we expect a similar $V_c - r$ - curve for NMR and µ-CT for the larger pore radii. If we assume a coincidence of the two curves at V_c = 0.5 we get a surface relaxivity of ρ = 54 µm/s.

The relaxation time distribution derived from SIP is attributed to a range of pore radii between 0.1 and 10 µm. We assume that the IP signals are caused by the ion-selected active zones in the narrow pores that are comparable with the pore throats. Therefore, we take the values of V_c at the minimum and maximum radius from the MIP curve. This procedure results in fair agreement between SIP and MIP curves in the relevant range of pore radii. In comparison with MIP, a slight overestimation of V_c is observed for pore radii larger than 0.3 µm.

The slope (s) of the curve log (V_c) versus log (r) is related to the fractal dimension D of the pore volume ($D = 3 - s$) [3]. We observe a varying slope in the investigated range of pore radii. The only range of more or less constant slope, which extends from pore radius 0.1 µm to 10 µm, corresponds to a fractal dimension D = 2.678 from MIP or D = 2.618 from SIP.

The measured porosity values as well as the ranges of pore radii of the used methods are compiled in Table 1. Different methods are characterized by different resolution, and the resulting porosities depend on the resolution.

Table 1: Measured porosity and pore radii range of sample BH5-2.

Methods	*r_min*	*r_max*	recognized porosity
	µm	µm	%
µ-CT	1.1	114	18.4
MIP	0.002	45	23.8
NMR	0.001	324	22.8
SIP	0.1	10	

CONCLUSIONS

The pore size distribution of Bentheimer sandstone can be determined by various methods (MIP, µ-CT, NMR, SIP) with different resolutions. The dominant pore throat radius of Bentheimer sandstone determined by MIP is about 14 µm. The µ-CT indicates a dominant pore body radius of about 47 µm. Because of the missing resolution for pore radii smaller than 1.75 µm, µ-CT underestimates the pore volume and porosity. NMR and µ-CT provide a similar pore radius distribution for larger pores if a surface relaxivity of 54 µm/s is selected. Only a restricted range of pore radii (0.1 µm to 10 µm) can be resolved by SIP. The methods µ-CT and NMR indicate the distribution of pore body radii, while MIP and SIP represent the distribution of pore throat radii. Comparing the two distributions, an average ratio between the radii of pore body to pore throat of about three has been determined for the investigated sample of Bentheimer sandstone. The $V_c - r$ curves has proved to be suitable for a comparison of the pore radii distribution resulting from the different methods. Our study shows that a good agreement between the pore radii distributions can only be achieved if the curves are adjusted considering the resolution and pore volume in the relevant range of pore radii. The MIP curve with the widest range in resolution should be used as reference.

ACKNOWLEDGEMENTS

The authors thank Sven Nordsiek for the Debye decomposition of the SIP data and Mike Müller-Petke for the acquisition of the NMR spectra for this study.

REFERENCES

1. Meyer, K., P. Klobes, and B. Röhl-Kuhn, 1997, *Certification of reference material with special emphasis on porous solids*: Crystal Research and Technol., **32**, 173-183.
2. Rouquerol, J., D. Avnir, D. C. W. Fairbridge, D. H. Everett, J. H. Haynes, N. Pernicone, J. D. F. Ramsay, K. S. W. Sing, and K. K. Unger, 1994, *Recommendations for the characterization of porous solids (Technical Report)*: Pure and Appl. Chem., **66**, 1739-1758.
3. Zhang, Z., and A. Weller, 2014, *Fractal dimension of pore space geometry of an Eocene sandstone formation*: Geophysics, **79**, D377-387. doi:10.1190/GEO2014-0143.1.
4. Rübner, K., and D. Hoffmann, 2006, *Characterization of mineral building materials by mercury-intrusion porosimetry*: Particle and Particle Systems Characterization, **23**, 20-28.
5. Weller, A., S. Nordsiek, and W. Debschütz, 2010, *Estimating permeability of sandstone samples by nuclear magnetic resonance and spectral-induced polarization*: Geophysics, **75**, E215 – E226. doi: 10.1190/1.3507304.
6. Schmitt, M., M. Halisch, C. Müller, and C. P. Fernandes, 2015, *Classification and quantification of pore shapes in sandstone reservoir rocks with 3-D X-ray micro-computed tomography*, Solid Earth Discuss., **7**, 3441-3479. doi:10.5194/sed-7-3441-2015.
7. Kruschwitz, S. F., A. Binley, D. Lesmes, and A. Elshenawy, 2010, *Textural controls on low-frequency electrical spectra of porous media*: Geophysics, **75**, 4, WA113–WA123.
8. Halisch, M., Schmitt, M., and Fernandes, Celso Peres, 2016, *Pore Shapes and Pore Geometry of Reservoirs Rocks from µ-CT Imaging and Digital Image Analysis*: Proceedings of the Annual Symposium of the SCA 2016, Snowmass, Colorado, USA, SCA2016-093.
9. Washburn, E. W., 1921, *The dynamics of capillary flow*: Physical Review, **17**, 3, 273-283.
10. Mancuso, C., C. Jommi, and F. D'Onza, 2012, *Unsaturated Soils: Research and Applications*, Volume 1, 123-130. doi: 10.1007/978-3-642-31116-1, ISBN: 978-3-642-31115-4 (Print).
11. Nordsiek, S., and A. Weller, 2008, *A new approach to fitting induced-polarization spectra*: Geophysics, **73**, 6, F235-F245. doi: 10.1190/1.2987412.
12. Schwarz, G., 1962, *A theory of the low-frequency dielectric dispersion of colloidal particles in electrolyte solution*: Journal of Physical Chemistry, **66**, 2636-2642. doi: 10.1021/j100818a067.
13. Revil, A., K. Koch, and K. Holliger, 2012, *Is it the grain size or the characteristic pore size that controls the induced polarization relaxation time of clean sands and sandstones?*: Water Resources Research, **48**, W05602. doi: 10.1029/2011WR011561.

14. Weller, A., Z. Zhang, L. Slater, S. Kruschwitz, and M. Halisch, 2016, *Induced polarization and pore radius – a discussion*: Geophysics, **81**, 5, D519-526. doi:10.1190/GEO2016-0135.1.
15. Revil, A., 2013, *Effective conductivity and permittivity of unsaturated porous materials in the frequency range 1 mHz-1GHz*: Water Resources Research, **49**, 306-327. doi: 10.1029/2012WR012700.
16. Schleifer, N., A. Weller, S. Schneider, and A. Junge, 2002, *Investigation of a Bronze Age plankway by spectral induced polarization*: Archeological Prospection, 9, 243–253. doi: 10.1002/arp.194.
17. Zimmermann, E., A. Kemna, J. Berwix, W. Glaas, and H. Vereecken., 2008, *EIT measurement system with high phase accuracy for the imaging of spectral induced polarization properties of soils and sediments*: Measurement Science and Technology, **19**, 9, 094010. doi: 10.1088/0957-0233/19/9/094010.
18. Dubelaar, W.C., and T. G. Nijland, 2015, *The Bentheim Sandstone: geology, petrophysics, varieties and its use as dimension stone*. In: Lollino, G., Giordan, D., Marunteanu, C., Christaras, B., Yoshinori, I., Margottini, C. (Eds.), *Engineering Geology for Society and Territory*, Springer International Publishing, Switzerland, **8**, 557-563.
19. Weller A., Y. Ding, Z. Zhang, M. Kassab, and M. Halisch, 2016, *Fractal dimension of pore space in carbonate samples from Tushka Area (Egypt)*: Proceedings of the Annual Symposium of the SCA 2016, Snowmass, Colorado, USA, SCA2016-085.